BeBeC-2020-D28

MORE THAN MICROPHONES – ALTERNATIVE SENSORS FOR BEAMFORMING IN AEROACOUSTICS?

Stefan Kröber[1] and Moritz Merk[2]

[1]R&D-Engineer Aeroacoustics & Aerodynamics
Daimler AG, 71059, Sindelfingen, Germany

[2]Master student
Daimler AG, 71059, Sindelfingen, Germany

ABSTRACT

The phased microphone array technique is a well established tool in aeroacoustic testing for the localization and quantification of sound sources. The measurements are almost exclusively carried out using microphones as array sensors. The underlying study evaluates the beamforming performance of alternative array sensors for aeroacoustic testing for automotive applications. In a first step, the thermal (scalar quantities: density, temperature, pressure) and kinematic (vector quantities: particle displacement, velocity, acceleration) sound field quantities are analyzed with respect to their measurability and their potential for the beamforming process. Resulting from this investigation, the acoustic velocity shows promising characteristics as an alternative to the state-of-the-art pressure sensors. In a second step, a simulation scenario was set up in order to compare the beamforming performance of the various alternative sensor arrays with a microphone array as reference. A systematic comparison was carried out examining the different point spread functions and their properties (MSR, resolution).

1 INTRODUCTION

The phased microphone array has become a widely used tool in aeroacoustic testing for the localization and quantification of sound sources. In aviation, this measurement technique is often employed on scaled models of aircrafts or aircraft components requiring measurements far above of the human range of audibility. In the case of a 1:10 scaled model, this would require measurements up to 160 kHz to cover the range of audibility and in order to ensure acoustic similarity in terms of the Helmholtz-number. In the automotive industry, the car development takes place using full-scale models or real cars that limits the frequency range requirements of a measurement to the range of audibility (16 Hz to 16000 Hz). Both, in aviation and in the

automotive industry the measurements are almost exclusively carried out using microphones as array sensors. For example, in the aeroacoustic wind tunnel of the Mercedes-Benz AG three microphone arrays, using all together 360 microphones, are installed for the aeroacoustic car development (see fig. 1).

Fig. 1: The aeroacoustic wind tunnel of the Daimler AG. Two side and one top microphone array employing 360 microphones all together are used for the aeroacoustic car development [6].

The underlying study evaluates the beamforming performance of alternative array sensors for aeroacoustic testing focusing on automotive applications within the range of audibility. In the context of this framework, section 2 examines the sound field quantities in terms of measurability in aeroacoustic testing and its possible benefits for beamforming. After that, the derivation of the various beamformers using different sensors and sensor combinations is given (section 3). An analytical test case using a line sensor array reveals the characteristic properties of the various employed beamformers (section 4). In the section 5, the test case is extended to 2-dimensional sensor array and an analysis of the simulation results is performed.

2 SOUND FIELD QUANTITIES

In this section, the question is clarified which sound field variables are measurable in principle and can contribute to a possible performance increase for the beamforming process. Since in aeroacoustic beamforming applications the measurements are almost exclusively carried out using microphones the acoustic pressure p' is used as a reference quantity below.

2.1 Thermodynamic quantities of sound fields

The thermodynamics of sound fields comprises the physical scalar quantities [7]: acoustic pressure fluctuations p', acoustic temperature T' and density fluctuations ρ'. The corresponding

static variables are given by p_0, T_0 and ρ_0. Provided that the ideal gas equation is valid (this assumption is reasonable for dry air) the linearized pressure-density relationship results for an isentropic process to

$$\frac{p'}{p_0} = \kappa \frac{\rho'}{\rho_0} \tag{1}$$

Furthermore the relative sound temperature is given by

$$\frac{p'}{p_0} = \frac{\kappa}{\kappa - 1} \frac{T'}{T_0} \tag{2}$$

Obviously, acoustic pressure, density and temperature fields have the same time and spatial dependence, apart from scaling factors. Considering the hypothetical case that density and temperature sensors would be available for measuring sound fields, it would only make sense to replace the microphones in an array by density or temperature sensors, when these sensors are more accurate, more robust, cheaper, easier to handle or have advantages in terms of the sensor directivity compared with microphones since these sensors do not provide more information about the sound field than microphones. Otherwise that there would be no additional benefit for the beamforming process by using density or temperature sensors instead of microphones. To the author's knowledge, currently, there are no practical acoustic density sensors available for the use in industrial applications in large wind tunnels. In the area of fundamental aeroacoustic research Panda and Seasholtz [8, 9] measured simultaneously acoustic density and velocity fluctuations of jet plumes using a recently developed non-intrusive point measurement technique based on molecular Rayleigh scattering. The technique uses a continuous-wave narrow line-width laser, Fabry–Perot interferometer and photon counting electronics.

Acoustic temperature fluctuations can be measured by using hotwires, but normally hotwires are used for the indirect determination of the acoustic particle velocity. An example is the acoustic particle velocity sensor from Microflown [10]. Another method, the coherent particle velocity method (CPV) [11], bases on the cross-correlation of two hotwire signals, allowing to measure the coherent particle velocity of the emitted sound waves. This method was used for the quantification of trailing edge noise whereas the hotwires were placed in the vicinity of the trailing edge in the flow. These methods will be readopted in next section when considering the kinematic quantities of sound fields like the acoustic particle velocity vector.

2.2 Kinematic quantities of sound fields

The kinematic quantities of sound fields comprise the physical quantities [7]: acoustic particle displacement, acoustic particle velocity and acoustic particle acceleration. In contrast to the thermal quantities, the kinematic quantities are vector fields. In addition to the amplitude information, these fields contain the additional information about the direction of propagation of the sound waves. Compared to the acoustic fields of the thermal quantities, the kinematic ones therefore have more information. For the beamforming process, the use of the kinematic quantities might accordingly be leading to a performance increase. The acoustic particle velocity vector can be measured employing acoustic vector sensors (AVS). To the author's

knowledge, a practical direct measurement of the acoustic particle displacement and acceleration is currently not possible. These quantities are typically determined by integration or differentiation of the acoustic particle velocity vector.

In the area of sonar, Nehorai and Paldi, [1], came up with the idea in the early 1990s to use acoustic vector sensors (AVS) for direction-of-arrival (DOA) estimation. In comparison to scalar sensors (pressure sensors), the output of an AVS consists of a vector of measurement signals. In particular, the combined measurement of pressure and acoustic velocity at a single measuring point was examined. The vectorial character of the acoustic velocity field provides additional information and has led to an improvement in the properties of the method. For example, when using a linear towed array of vector sensors instead of pressure sensors to determine the location of surface ships, the left/right ambiguity problem does not arise, avoiding the need to rotate the vessel through 90° between readings. Based on this publication, numerous investigations of the influence of this new measurement sensor system were carried out in the area of the sonar. Hochwald and Nehorai, [2], for example, investigated the source localization properties of AVS compared to conventional pressure sensors. New beamforming algorithms for the use of AVS have also been investigated, for example, by Kitchens, [3], or Hawkes and Nehorai [4].

In the field of aeroacoustics, pressure sensors are almost exclusively used for beamforming. Fernandez Comesana et al., [5], was the first publication in 2017 in which AVS are used for aeroacoustic measurements. The low-frequency sound field generated by a wind turbine was measured employing AVS from Microflown [10] being able to measure all three acoustic particle velocity components and the sound pressure. Such an AVS is depicted in figure 2. On the one hand, they have demonstrated that AVS based beamforming can be performed under harsh and windy condition in practical applications. On the other hand, this publication performs no systematic comparison between an AVS array with a classic microphone array. Therefore, the underlying study evaluates the beamforming performance of AVS for aeroacoustic testing focusing on automotive applications using full scale models in wind tunnel tests.

Fig. 2: The Acoustic vector sensor from Microflown [10] can measure all three components of the acoustic particle velocity and the sound pressure (frequency range: 20 – 20000 Hz).

3 BEAMFORMING WITH VARIOUS SENSORS

3.1 Conventional Beamforming using arbitrary sensors

The present study applies the widely used conventional beamforming (CB) using the source model $\hat{y}$ [12]. The complex amplitudes $\hat{a}$ of the sources at the location ξ can be estimated by comparing the measured signal vector **y** (acoustic pressure and/or acoustic particle velocity) with the steering vector **g** (monopole assumption). An often used approach to determine $\hat{a}$ is through minimization. This leads to the following equations:

$$\hat{y}(\boldsymbol{x}, \boldsymbol{\xi}, f) = \hat{a}(f)\boldsymbol{g}(\boldsymbol{x}, \boldsymbol{\xi}, f) \tag{3}$$

$$J = \|\boldsymbol{y} - \hat{a}\boldsymbol{g}\|^2 \tag{4}$$

$$\hat{a} = \frac{\boldsymbol{g}^H \boldsymbol{y}}{\|\boldsymbol{g}\|^2} \tag{5}$$

$$B = \frac{|\hat{a}|^2}{2} = \frac{1}{2}\frac{\boldsymbol{g}^H \boldsymbol{y}\boldsymbol{y}^H \boldsymbol{g}}{\|\boldsymbol{g}\|^4} = \frac{\boldsymbol{g}^H \boldsymbol{C}\boldsymbol{g}}{\|\boldsymbol{g}\|^4} \tag{6}$$

Equation (6) denotes the beamformer output as the solution of the minimization with *C* as cross-spectral matrix and $(.)^H$ denotes the complex conjugate transpose.

3.2 Conventional Beamforming using pressure and acoustic particle velocity sensors

In the following, the specific formulations of conventional beamforming from the previous section are derived and listed for the use of the different measuring sensors. All in all three different processes are considered:

1. The standard CB method employing pressure sensors will be used as a reference.
2. A CB method using n-dimensional acoustic particle velocity sensors ($n \in \{1, 2, 3\}$).
3. A CB method using the combination of pressure sensors and 3-dimensional acoustic particle velocity sensors, whereas the measurement signals of the sound pressure and the acoustic particle velocity sensors will be independently of one another processed in the beamforming process.

3.2.1 Conventional Beamforming with acoustic pressure sensors

In the case of using an array consisting of k pressure sensors and combines that with the monopole assumption as possible source one obtains for the steering vector:

$$\boldsymbol{g_p} = \begin{bmatrix} g_{p,1} & \cdots & g_{p,k} & \cdots & g_{p,M} \end{bmatrix}^T$$
$$g_{p,k} = \frac{1}{4\pi d_k} e^{-j\omega\frac{d_k}{c}}. \tag{7}$$

$d_k = ||\boldsymbol{x_k} - \boldsymbol{\xi}||$ denotes the distance between an assumed source position and the k-sensor. The measured complex pressure signal vector in the frequency domain is given by $\boldsymbol{y_p} \in \mathbb{C}^{M\times 1}$whereas M denotes the number of employed sensors.

3.2.2 Conventional Beamforming with acoustic particle velocity sensors

In the following the description of the CB using n-dimensional acoustic particle velocity sensors $CB_{v,nD}$ () is presented. The given description applies regardless of whether the acoustic particle velocity is measured in one (1D), two (2D) or three (3D) spatial directions. The single measuring directions are only assumed orthogonal to each other. The exact number of measuring directions used are identified within the name $CB_{v,nD}$ by the index $(.)_{nD}$ ($n \in \{1, 2, 3\}$). The measured complex signal vector of the acoustic particle velocity in the frequency domain is given by

$$\boldsymbol{y}_{v,nD} = \left[\boldsymbol{y}_{v,nD,1}{}^{T} \quad \cdots \quad \boldsymbol{y}_{v,nD,k}{}^{T} \quad \cdots \quad \boldsymbol{y}_{v,nD,M}{}^{T}\right]^{T} \in \mathbb{C}^{nM\times 1} \tag{8}$$

with $\boldsymbol{y}_{v,nD,k} \in \mathbb{C}^{n\times 1}$. Furthermore one obtains for the steering vector by using eq. (5)

$$\begin{aligned} \boldsymbol{g}_{v,nD} &= \left[\boldsymbol{g}_{v,nD,1}{}^{T} \quad \cdots \quad \boldsymbol{g}_{v,nD,k}{}^{T} \quad \cdots \quad \boldsymbol{g}_{v,nD,M}{}^{T}\right]^{T} \\ \boldsymbol{g}_{v,nD,k} &= -\frac{1}{\rho_0 c}\left[1 - j\frac{c}{\omega d_k}\right]\frac{1}{4\pi d_k} e^{-j\omega\frac{d_k}{c}}\boldsymbol{u}_{nD,k}. \end{aligned} \tag{9}$$

$\boldsymbol{u}_{nD,k}$ represents the normalized and into the measuring space projected direction vector between the position of the k-th sensor and any evaluation position.

3.2.3 Conventional Beamforming with acoustic pressure and acoustic particle velocity sensors

This section describes the CB using the acoustic pressure and the acoustic particle velocity. This approach uses both quantities, but independently. Therefore, the notation $CB_{p,v,nD}$ is used for this method. For the case of a plane waves this beamforming method is described for example in Hawkes and Nehorai [10] for sonar applications. In the current study this method is extended to monopoles as assumed sources. As a result of the different orders of magnitude of the sound pressure and the sound velocity, the individual measurement signals cannot be simply arranged one after the other in the signal vector $\boldsymbol{y}_{p,v,nD,k} \in \mathbb{C}^{[(n\times 1)M]\times 1}$. In order to be able to establish comparability between the measured values, they have to be firstly normalized to the same order of magnitude. This normalization is also applied to the entries of the weighting vector $\boldsymbol{g}_{p,v,nD,k} \in \mathbb{C}^{[(n\times 1)M]\times 1}$. The following normalized vectors are introduced:

$$\begin{aligned} \tilde{\boldsymbol{y}}_p &= \frac{\boldsymbol{y}_p}{\|\boldsymbol{g}_p\|} \\ \tilde{\boldsymbol{g}}_p &= \frac{\boldsymbol{g}_p}{\|\boldsymbol{g}_p\|} \end{aligned} \tag{10}$$

and

$$\begin{aligned} \tilde{\boldsymbol{y}}_{v,nD} &= \frac{\boldsymbol{y}_{v,nD}}{\|\boldsymbol{g}_{v,3D}\|} \\ \tilde{\boldsymbol{g}}_{v,nD} &= \frac{\boldsymbol{g}_{v,nD}}{\|\boldsymbol{g}_{v,3D}\|}. \end{aligned} \tag{11}$$

It should be noted here that when using n acoustic particle velocity components, the normalization of the measured signal vector $\boldsymbol{y}_{v,nD}$ or the weighting vector $\boldsymbol{g}_{v,nD}$ is always performed by means of the 3D weighting vector $\boldsymbol{g}_{v,3D}$. This procedure ensures that the complete velocity vector (3D) is always weighted in the same way as the corresponding signal of the pressure. In 1D and 2D cases, this leads to a reduction of the influence of the measurement signals of the acoustic particle velocity by the factor $||\boldsymbol{u}_{v,nD}||$. The measured signal vector $\boldsymbol{y}_{p,v,nD}$ and the weighting vector $\boldsymbol{p}_{p,v,nD}$ are finally composed of the normalized quantities of eq. (10) and (11) together

$$\begin{aligned} \boldsymbol{y}_{p,v,nD} &= \begin{bmatrix} \tilde{\boldsymbol{y}}_p{}^T & \tilde{\boldsymbol{y}}_{v,nD}{}^T \end{bmatrix}^T \\ \boldsymbol{g}_{p,v,nD} &= \begin{bmatrix} \tilde{\boldsymbol{g}}_p{}^T & \tilde{\boldsymbol{g}}_{v,nD}{}^T \end{bmatrix}^T \end{aligned} \tag{12}$$

The source strength results from the combination of eq. (5) and (12) to

$$\begin{aligned} \hat{a}_{p,v,nD} &= \frac{\boldsymbol{g}_{p,v,nD}{}^H \boldsymbol{y}_{p,v,nD}}{\|\boldsymbol{g}_{p,v,nD}\|^2} \\ &= \frac{1}{\|\boldsymbol{g}_{p,v,nD}\|^2} \left(\tilde{\boldsymbol{g}}_p{}^H \tilde{\boldsymbol{y}}_p + \tilde{\boldsymbol{g}}_{v,nD}{}^H \tilde{\boldsymbol{y}}_{v,nD} \right) \\ &= \frac{1}{1 + \frac{\|\boldsymbol{g}_{v,nD}\|^2}{\|\boldsymbol{g}_{v,3D}\|^2}} \left(\underbrace{\frac{\boldsymbol{g}_p{}^H \boldsymbol{y}_p}{\|\boldsymbol{g}_p\|^2}}_{\hat{a}_p} + \underbrace{\frac{\boldsymbol{g}_{v,nD}{}^H \boldsymbol{y}_{v,nD}}{\|\boldsymbol{g}_{v,nD}\|^2}}_{\hat{a}_{v,nD}} \frac{\|\boldsymbol{g}_{v,nD}\|^2}{\|\boldsymbol{g}_{v,3D}\|^2} \right). \end{aligned} \tag{13}$$

The resulting source strength $\hat{a}_{p,v,nD}$ is a weighted mean value from the approximated source strengths $\hat{a}_p$ and $\hat{a}_{v,nD}$.
The original approach of Hawkes and Nehorai [10] assumes plane waves and employs the acoustic impedance of plane waves $\rho_0 c$ for the normalization of the measured signal and weighting vector which results to

$$\begin{aligned} \boldsymbol{g}_{p,v,nD} &= \begin{bmatrix} \boldsymbol{g}_p{}^T & \rho_0 c\, \boldsymbol{g}_{v,nD}{}^T \end{bmatrix}^T \\ \boldsymbol{y}_{p,v,nD} &= \begin{bmatrix} \boldsymbol{y}_p{}^T & \rho_0 c\, \boldsymbol{y}_{v,nD}{}^T \end{bmatrix}^T. \end{aligned} \tag{14}$$

If these formulations are included in the solution of the minimization problem of the CB (eq. 5) one accordingly obtains

$$\begin{aligned}\hat{a}_{p,v,nD} &= \frac{1}{\|\boldsymbol{g_p}\|^2 + (\rho_0 c)^2 \|\boldsymbol{g_{v,nD}}\|^2} \left(\boldsymbol{g_p}^H \boldsymbol{y_p} + (\rho_0 c)^2 \boldsymbol{g_{v,nD}}^H \boldsymbol{y_{v,nD}} \right) \\ &= \frac{1}{1 + \frac{(\rho_0 c)^2}{\|\boldsymbol{g_p}\|^2} \|\boldsymbol{g_{v,nD}}\|^2} \left(\frac{\boldsymbol{g_p}^H \boldsymbol{y_p}}{\|\boldsymbol{g_p}\|^2} + \frac{(\rho_0 c)^2}{\|\boldsymbol{g_p}\|^2} \boldsymbol{g_{v,nD}}^H \boldsymbol{y_{v,nD}} \right) \\ &= \frac{1}{1 + \frac{\|\boldsymbol{g_{v,nD}}\|^2}{\|\boldsymbol{g_{v,3D}}\|^2}} \left(\frac{\boldsymbol{g_p}^H \boldsymbol{y_p}}{\|\boldsymbol{g_p}\|^2} + \frac{\boldsymbol{g_{v,nD}}^H \boldsymbol{y_{v,nD}}}{\|\boldsymbol{g_{v,3D}}\|^2} \right).\end{aligned} \tag{15}$$

Taking into account that if the observer is far away from of the monopole source the wave fronts can be considered as plane waves and subsequently holds

$$\|\boldsymbol{g_{v,3D}}\| = \frac{\|\boldsymbol{g_p}\|^2}{(\rho_0 c)^2} \tag{16}$$

It is obviously by using eq. (16) that eq. (13) and eq. (15) coincide with each other in the far field case, as one would expected.

4 ANALYTICAL TEST CASE

In this section, analytical solutions of the individual beamforming algorithms described in section 3 are derived. In a first step, the derivation is performed for any array geometry under the assumptions described in the further course of this section. Due to the analogous approach in the following derivation for all examined beamforming algorithms, in the following, this will be carried out only once, representatively on the basis of the CB_p. The solutions of the remaining CB processes are listed only. The complete derivation is given in the appendix A and B. Figure 3 shows the used coordinate system.

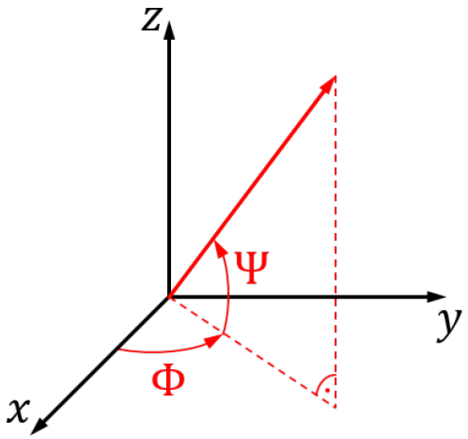

Fig. 3: Employed coordinate system.

4.1 Assumptions of the analytical test case

The derivation of the analytical solutions bases on the following assumptions:

1. The arrays consists of a number of M sensors.
2. The distance between the source/arbitrary assumed source positions and array is much larger than the array diameter D_A:

$$\begin{aligned} d_{0,k} &= \|\boldsymbol{x_k} - \boldsymbol{\xi_0}\| \\ d_{0,k} &\gg D_A \qquad ,\forall k = 1, ..., M. \\ \frac{1}{d_{0,k}} &= \frac{1}{d_0} \qquad ,\forall k = 1, ..., M. \\ d_k &\gg D_A \qquad \forall k = 1, ..., M \\ \frac{1}{d_k} &= \frac{1}{d} \qquad ,\forall k = 1, ..., M \end{aligned} \tag{17}$$

3. The incoming wave fronts can be considered as plane waves

$$\begin{aligned} \Phi_{0,k} &= \Phi_0 \qquad ,\forall k = 1, ..., M \\ \Psi_{0,k} &= \Psi_0 \qquad ,\forall k = 1, ..., M \\ \Phi_k &= \Phi \qquad ,\forall k = 1, ..., M \\ \Psi_k &= \Psi \qquad ,\forall k = 1, ..., M \end{aligned} \tag{18}$$

and subsequently, there is approximately no phase difference between the pressure and the acoustic particle velocity:

$$\begin{aligned} 1 - j\frac{c}{\omega d_{0,k}} &\approx 1 \qquad ,\forall k = 1, ..., M \\ 1 - j\frac{c}{\omega d_k} &\approx 1 \qquad ,\forall k = 1, ..., M. \end{aligned} \tag{19}$$

4.2 Analytical solution for Conventional Beamforming using the pressure CB_p

The combination of the made assumptions leads to the CB_p-weighting vector elements

$$g_{p,k} = \frac{1}{4\pi d} e^{j\varphi_k}. \tag{20}$$

φ_k denotes the corresponding phase. Furthermore one obtains

$$\|\boldsymbol{g_p}\|^2 = \boldsymbol{g_p}^H \boldsymbol{g_p} = \sum_{k=1}^{M} (g_{p,k})^* g_{p,k} = \frac{M}{(4\pi d)^2} \tag{21}$$

$$\boldsymbol{g_p}^H \boldsymbol{y_p} = \boldsymbol{g_p}^H a \boldsymbol{g_{p,0}} \quad = \frac{a}{(4\pi)^2 d d_0} \sum_{k=1}^{M} e^{j(\varphi_{0,k} - \varphi_k)}$$

Assuming a single source and no disturbances the beamforming solution results to

$$B_p = \frac{1}{2}|\hat{a}|^2 = \frac{|a|^2}{2} \left| \frac{\boldsymbol{g_p}^H \boldsymbol{g_{p,0}}}{\|\boldsymbol{g_p}\|^2} \right|^2 = \frac{|a|^2}{2} \left(\frac{d}{d_0} \right)^2 \underbrace{\frac{1}{M^2} \left| \sum_{k=1}^{M} e^{j(\varphi_{0,k} - \varphi_k)} \right|^2}_{|W_p|^2}. \tag{22}$$

W_p denotes the so-called aperture 'aperture smoothing function' (ASF) [13].

4.3 Analytical solution for Conventional Beamforming using the acoustic particle velocity $CB_{n,vD}$

Following the same procedure as before for the acoustic pressure, one obtains

$$\begin{aligned} B_{v,nD} = & \frac{|a|^2}{2} \left(\frac{d}{d_0} \right)^2 \frac{1}{M^2} {A_{v,nD}}^2 \left| \sum_{k=1}^{M} e^{j(\varphi_{0,k} - \varphi_k)} \right|^2 \\ = & \frac{|a|^2}{2} \left(\frac{d}{d_0} \right)^2 {A_{v,nD}}^2 |W_p|^2 \\ \models & {A_{v,nD}}^2 \, B_p \end{aligned} \tag{23}$$

$$A_{v,nD} = \frac{\boldsymbol{u_{nD}}^T \boldsymbol{u_{0,nD}}}{\|\boldsymbol{u_{nD}}\|^2}$$

The complete derivation is given in the appendix A. According to eq. (23) under the made assumptions in eq. (17-19), the $CB_{n,vD}$-PSF consists of the PSF of the CB_p and an additional amplitude modulation term (AMT) $A_{v,nD}^2$. This results from the additional information of the vectorial field of the acoustic particle velocity compared to the scalar pressure field. The occurring ASF corresponds to that of the B_p W_p.

4.4 Analytical solution for Conventional Beamforming using the combination of acoustic pressure and the acoustic particle velocity $CB_{p,n,vD}$

$$\begin{aligned} B_{p,v,nD} &= \frac{|a|^2}{2}\left(\frac{d}{d_0}\right)^2 \frac{1}{M^2} {A_{p,v,nD}}^2 \left|\sum_{k=1}^{M} e^{j(\varphi_{0,k}-\varphi_k)}\right|^2 \\ &= \frac{|a|^2}{2}\left(\frac{d}{d_0}\right)^2 {A_{p,v,nD}}^2 |W_p|^2 \\ &= {A_{p,v,nD}}^2 \, B_p \end{aligned} \tag{24}$$

$$A_{p,v,nD} = \frac{1 + \boldsymbol{u_{nD}}^T \boldsymbol{u_{0,nD}}}{1 + \|\boldsymbol{u_{nD}}\|^2}$$

As in the case of $CB_{n,vD}$ the PSF of the $CB_{p,n,vD}$ consists of the ASF of the CB_p W_p and the AMT $A^2_{p,v,nD}$, which differs from that of the $CB_{n,vD}$. The complete derivation is given in the appendix B.

4.5 Analytical test case using a line array

In order to show the underlying characteristics of the various beamformers the following simple test case is considered. The array consists of $M = 10$ sensor arranged on a line having a constant sensor spacing δ. A single monopole source is located far away from the line array so that the assumptions in eq. (17-19) are fulfilled. Subsequently, the source direction is given by the angles $\Phi_0 = \pi/2$ and $\Psi = 0$. The source has the frequency $f = c/4\delta$ (c denotes the speed of sound). The corresponding ASF can be found in [13]

$$|W_p|^2 = \left(\frac{\sin\left(\frac{\omega M \delta}{2c}\right)}{\sin\left(\frac{\omega \delta}{2c}\right)}\right)^2 . \tag{25}$$

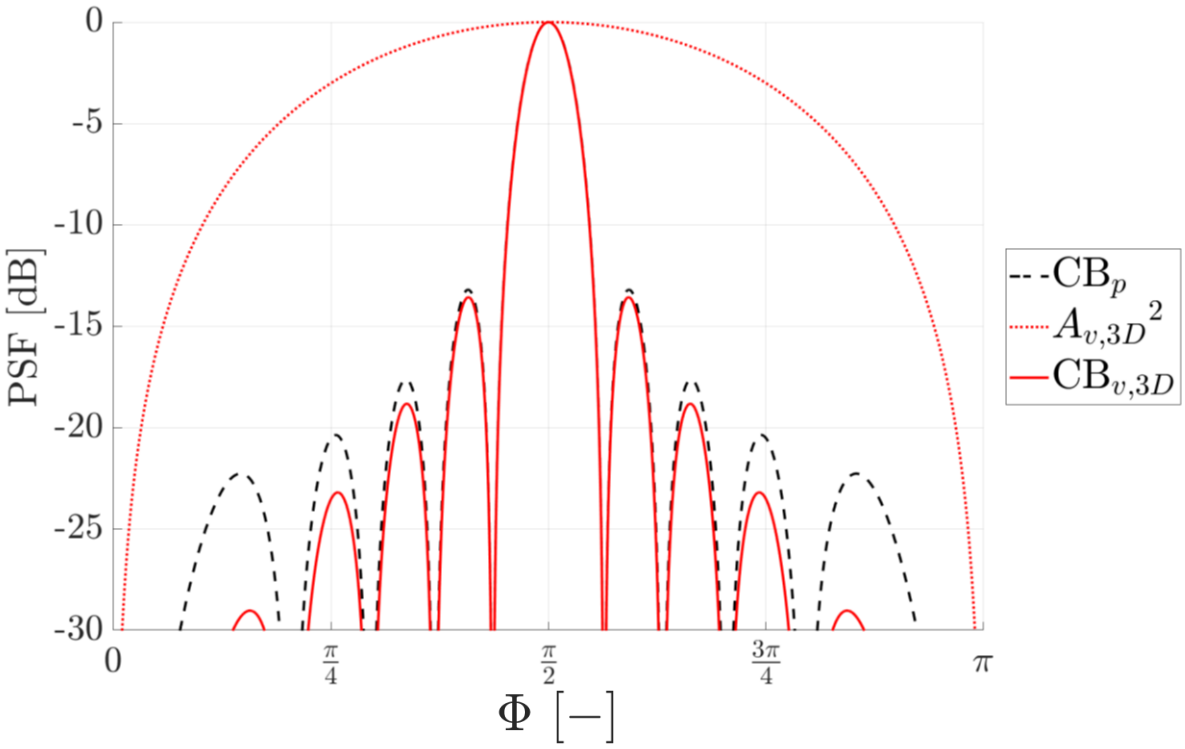

Fig. 4: Normalized PSF of the line array consisting of 10 sensors over the angle Φ for the beamforming approaches CB_p and $CB_{v,3D}$.

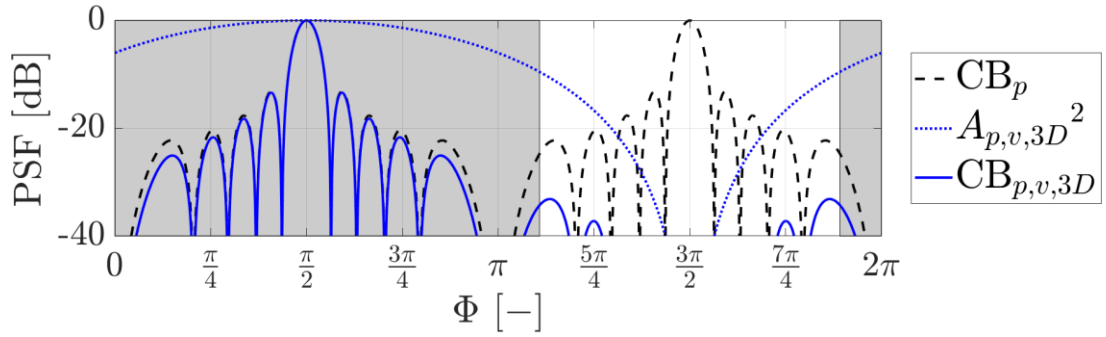

Fig. 5: Normalized PSF of the line array consisting of 10 sensors over the angle Φ for the beamforming approaches CB_p and $CB_{p,v,3D}$.

Figure 4 and 5 show the resulting beamformer outputs for the three different methods CB_p, $CB_{v,3D}$ and $CB_{p,v,3D}$. The modulation terms of $CB_{v,3D}$ and $CB_{p,v,3D}$ lead to an improvement of the main-to-side lobe ratio (MSR) compared to CB_p due to the resulting reduction of the corresponding side lobes. Both AMT's, $A^2_{v,nD}$ and $A^2_{p,v,nD}$, have their maximum values in the direction from which the sound waves are emitted and reach a value of one at this point. On the one hand this means that all considered CB scheme, in the case of a single source and no disturbances, result in the exact the calculation of the source strength. On the other hand the appearance of the main lobe does not change and thus, the resolution of all three beamforming methods is the same. In contrast to the CB_p-scheme the $\pi/2$ / $3\pi/2$-direction ambiguity problem does not arise in the case of $CB_{p,v,3D}$-method.

5 BEAMFORMING PERFORMANCE OF A 2-DIMENSIONAL ARRAY

The second test case uses a 2-dimensional sensor array consisting of M = 144 sensors, depicted in fig. 6. The widely used layout employs nine logarithmic spirals and has a diameter of 1m [14].

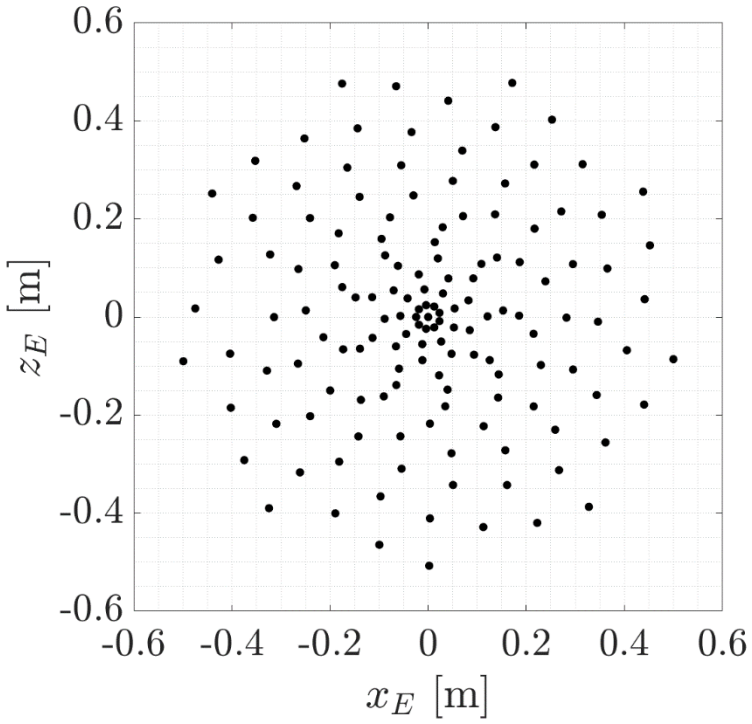

Fig. 6: Layout of the 2-dimensional sensor array.

The setup simulates a single monopole sound at the source location $\boldsymbol{\xi_0} = [0,\ 1.5\,m\,, 0\,m]$. The source evaluation comprises the area $\pm 2m$ in x- and z-direction each. The used frequency range in the simulation is $f \in [680\,Hz, 20400\,Hz]$ which corresponds to the Helmholtz-number range $He_D \in [2{,}60]$ using the definition

$$He_D = \frac{D_A}{\lambda} \tag{26}$$

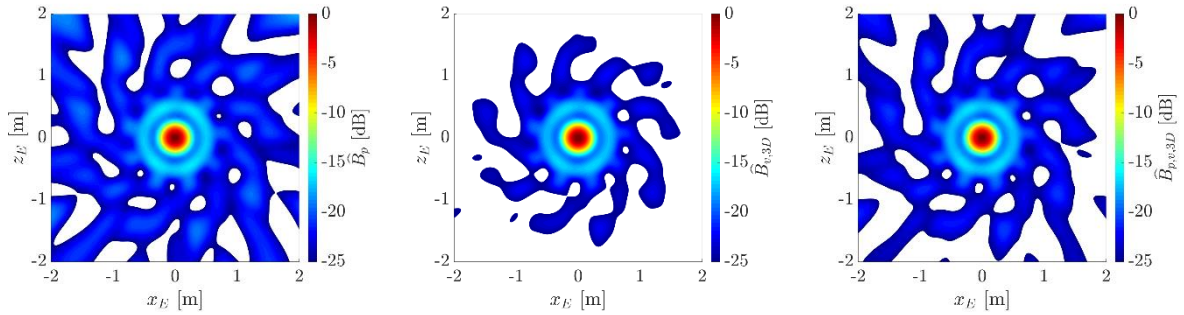

Fig. 7: Beamforming results of the 2-dimensional array for a simulated monopole for $He = 8$: CB_p (left), $CB_{v,3D}$ (middle), $CB_{p,v,3D}$ (right).

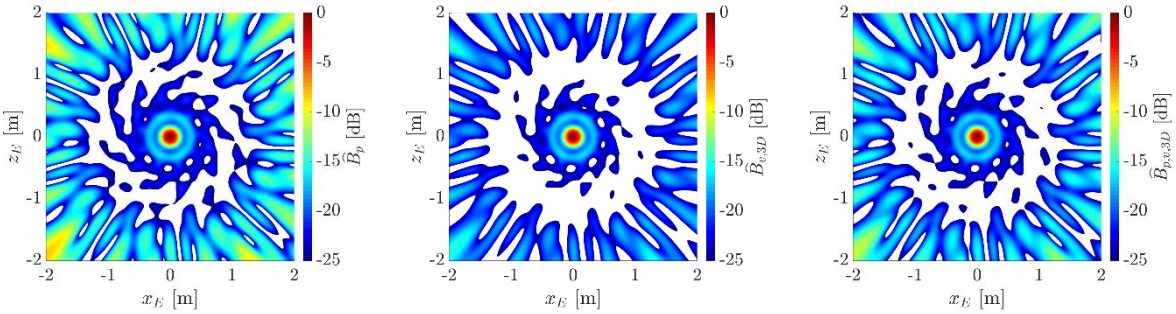

Fig. 8: Beamforming results of the 2-dimensional array for a simulated monopole for $He = 12$: CB_p (left), $CB_{v,3D}$ (middle), $CB_{p,v,3D}$ (right).

The beamforming results of the simulated monopole sound source for $He = 8$ und $He = 12$ are exemplarily depicted in fig. 7 and 8. The various source maps exhibit a very comparable main lobe appearance for all three different methods CB_p, $CB_{v,3D}$ and $CB_{p,v,3D}$. This is confirmed by plotting the normalized resolution (3dB bandwidth of the main lobe) in fig. 9. For the majority of the considered frequency range the resolution is nearly identical for all three examined beamforming methods. Differences appear in terms of the side lobes. As before in the analytical test case using the line sensor array the amplitude modulation term decreases the side lobes for $CB_{p,v,3D}$ and in particular for $CB_{v,3D}$ compared with the CB_p-approach. This can be seen over the complete frequency range as depicted in fig. 10. $CB_{v,3D}$ shows an improvement up to 7 dB and $CB_{p,v,3D}$ results in an improvement up to 4 compared with CB_p for the MSR.

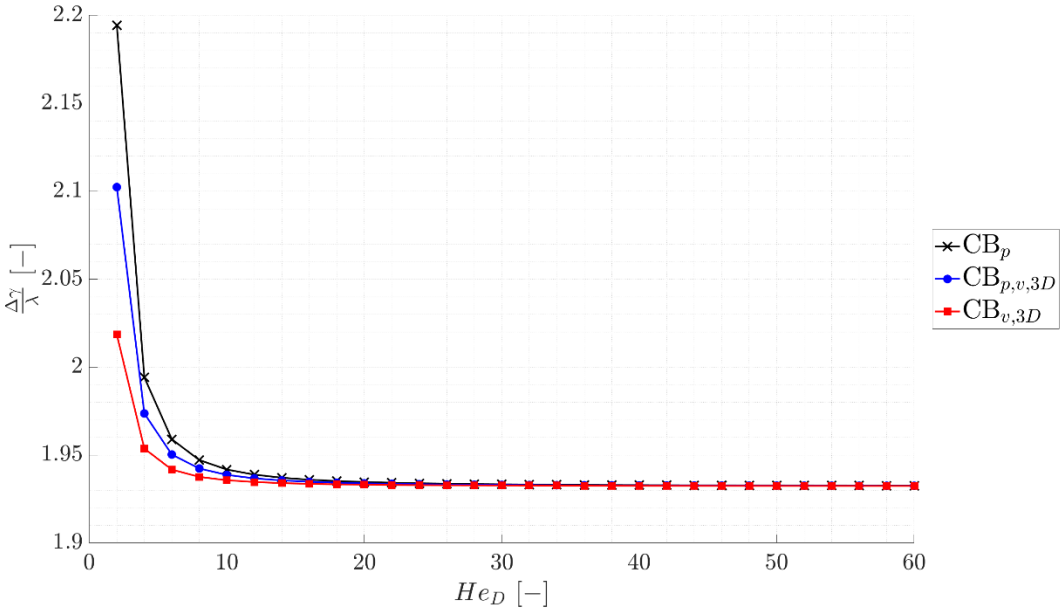

Fig. 9: With the wavelength normalized source resolution (3dB main lobe width) for all three different beamforming methods CB_p, $CB_{v,3D}$ and $CB_{p,v,3D}$.

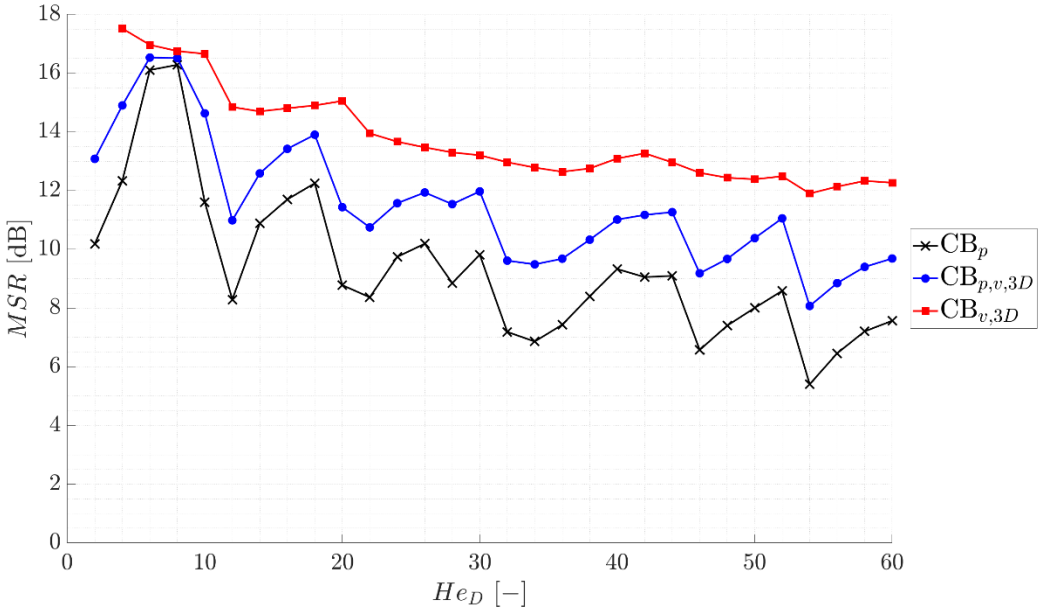

Fig. 10: Main-to-side lobe ratio for all three different beamforming methods CB_p, $CB_{v,3D}$ and $CB_{p,v,3D}$.

6 SUMMARY

The underlying study evaluates the beamforming performance of alternative array sensors for aeroacoustic testing for automotive applications. In a first step, the thermal (scalar quantities: density, temperature, pressure) and kinematic (vector quantities: particle displacement, velocity, acceleration) sound field quantities are analyzed with respect to their measurability and their potential for the beamforming process. Resulting from this investigation, the acoustic velocity shows promising characteristics as an alternative to the state-of-the-art pressure sensors in the range of audibility. In a second step, a simulation scenario was set up in order to compare the beamforming performance of a Conventional Beamforming using the acoustic particle velocity $CB_{v,3D}$ and a Conventional Beamformer using the combination of acoustic pressure and the acoustic particle velocity $CB_{p,v,3D}$ with a Conventional Beamforming using the acoustic pressure CB_p as reference. A systematic comparison was carried out examining the different point spread functions and their properties (MSR, resolution). The modulation terms of $CB_{v,3D}$ and $CB_{p,v,3D}$ lead to an improvement of the main-to-side lobe ratio (MSR) compared to CB_p due to the resulting reduction of the corresponding side lobes. The resolution of all three beamforming methods remains the same. In the future, it is worth looking at the properties of a beamformer that combines the acoustic particle velocity and the acoustic pressure to the acoustic intensity as relevant quantity since both can be measured by an acoustic vector sensor (AVS). Furthermore, the influence of disturbances occurring in aeroacoustic wind tunnels on the beamforming results should be examined in order to extend the present performance analysis.

REFERENCES

[1] A. Nehorai und E. Paldi: “Acoustic Vector-Sensor Array Processing.” IEEE Transactions on Signal Processing, Vol. 42, No. 9, p. 2481-2491, 1994.

[2] B. Hochwald und A. Nehorai: “Identifiability in Array Processing Models with Vector-Sensor Applications.” IEEE Transactions on Signal Processing, Vol. 44, No. 1, p. 83-95, 1996

[3] J. P. Kitchens: “Acoustic Vector-Sensor Array Processing.” PhD-Thesis, Massachusetts Institute of Technology, Cambridge, 2010.

[4] M. Hawkes and A. Nehorai: “Acoustic Vector-Sensor Beamforming and Capon Direction Estimation.” IEEE Transactions on Signal Processing, Vol. 46, No. 9, p. 2291-2304, 1998.

[5] D. Fernandez Comesana, K. Ramamohan, D. Perez Cabo and G. Carillo Pousa: “Modelling and localizing low frequency noise of a wind turbine using an array of acoustic vector sensors.” 7th International Conference on Wind Turbine Noise, 2017.

[6] R. Buckisch, H. Tokuno und H. Knoche: “The New Daimler Automotive Wind Tunnel: Acoustic Properties and Measurement System.” 10th FKFS Conference, 2015.

[7] Möser, M.: “Engineering Acoustics”, Second Edition, Springer, 2009

[8] Panda J., Seasholtz R.G.: “Experimental investigation of density fluctuations in high-speed jets and correlation with generated noise.” J. Fluid Mech. 450:97–130, 2002

[9] Panda J., Seasholtz R.G., Elam K.A.: “Investigation of noise sources in high-speed jets via correlation measurements.” J. Fluid Mech. 537:349–385, 2005

[10] https://www.microflown.com/products/standard-probes/

[11] Herrig, A., Wuerz, W., Lutz, T., Kraemer, E.: “Trailing-Edge Noise Measurements Using a Hot-Wire Based Coherent Particle Velocity Method”, AIAA 2006-3876

[12] P. Sijtsma.: “Experimental techniques for identification and characterisation of noise sources.” NLR-TP-2004-165, 2004.

[13] D. H. Johnson, D. E. Dudgeon: “Array Signal Processing - Concepts and Techniques.” PTR Prentice Hall, 1993.

[14] L. Koop: “Microphone-array processing for wind-tunnel measurements with strong background noise.” In 14th AIAA/CEAS Aeroacoustics Conference, AIAA-Paper 2008-2907,Vancouver, Canada, 2008.

A Appendix: Derivation of the analytical solution for Conventional Beamforming using the acoustic particle velocity $CB_{n,vD}$

$$\boldsymbol{g_{v,nD,k}} = -\frac{1}{4\pi\rho_0 cd} e^{j\Delta\varphi_k} \boldsymbol{u_{nD}} \tag{A.1}$$

$$\begin{aligned} \|\boldsymbol{g_{v,nD}}\|^2 &= \boldsymbol{g_{v,nD}}^H \boldsymbol{g_{v,nD}} \\ &= \sum_{k=1}^{M} \boldsymbol{g_{v,nD,k}}^H \boldsymbol{g_{v,nD,k}} \\ &= \frac{M}{(4\pi\rho_0 cd)^2} \|\boldsymbol{u_{nD}}\|^2 . \end{aligned} \tag{A.2}$$

$$\begin{aligned} \boldsymbol{g_{v,nD}}^H \boldsymbol{y_{v,nD}} &= a_m \, \boldsymbol{g_{v,nD}}^H \boldsymbol{g_{v,nD,0}} \\ &= \frac{a_m}{(4\pi\rho_0 c)^2} \frac{1}{dd_0} \underbrace{\left[\frac{\boldsymbol{u_{nD}}^H \boldsymbol{u_{nD,0}}}{\|\boldsymbol{u_{nD}}\|^2} \right]}_{A_{v,nD}} \sum_{k=1}^{M} e^{j(\Delta\varphi_{0,k} - \Delta\varphi_k)} \end{aligned} \tag{A.3}$$

$$\begin{aligned} B_{v,nD} &= \frac{1}{2} |\hat{a}_{v,nD}|^2 \\ &= \frac{|a_m|^2}{2} \left(\frac{d}{d_0} \right)^2 \frac{1}{M^2} A_{v,nD}^2 \left| \sum_{k=1}^{M} e^{j(\Delta\varphi_{0,k} - \Delta\varphi_k)} \right|^2 \\ &= \frac{|a_m|^2}{2} \left(\frac{d}{d_0} \right)^2 A_{v,nD}^2 |\Theta_p|^2 \\ &= A_{v,nD}^2 B_p. \end{aligned} \tag{A.4}$$

B Appendix: Derivation of the analytical solution for Conventional Beamforming using the acoustic particle velocity and the acoustic pressure $\boldsymbol{CB_{p,n,vD}}$

$$
\begin{aligned}
B_{p,v,nD} = & \frac{1}{2}\left|\hat{a}_{p,v,nD}\right|^2 \\
= & \frac{1}{2}\left(\frac{1}{1+\frac{\|\boldsymbol{g_{v,nD}}\|^2}{\|\boldsymbol{g_{v,3D}}\|^2}}\right)^2 \left\|\hat{a}_p + \hat{a}_{v,nD}\frac{\|\boldsymbol{g_{v,nD}}\|^2}{\|\boldsymbol{g_{v,3D}}\|^2}\right\|^2 \\
= & \frac{1}{2}\frac{1}{\left(1+\|\boldsymbol{u_{nD}}\|^2\right)^2}\left[a^2\left(\frac{d}{d_0}\right)^2\frac{1}{M^2}\left(1+(\boldsymbol{u_{nD}}^T\boldsymbol{u_{nD,0}})^2\right)\left|\sum_{k=1}^{M}e^{j\left(\Delta\varphi_{0,k}-\Delta\varphi_k\right)}\right|^2\right] \\
= & \frac{|a_m|^2}{2}\left(\frac{d}{d_0}\right)^2\frac{1}{M^2}\underbrace{\left[\frac{1+\boldsymbol{u_{nD}}^T\boldsymbol{u_{nD,0}}}{\left(1+\|\boldsymbol{u_{nD}}\|^2\right)^2}\right]^2}_{A_{p,v,nD}{}^2}\left|\sum_{k=1}^{M}e^{j\left(\Delta\varphi_{0,k}-\Delta\varphi_k\right)}\right|^2 \\
= & \frac{|a_m|^2}{2}\left(\frac{d}{d_0}\right)^2 A_{p,v,nD}{}^2\left|\Theta_p\right|^2 \\
= & A_{p,v,nD}{}^2 B_p.
\end{aligned}
\tag{B.1}
$$